Research Article J. Electrochem. Sci. Technol., **2018**, 9(4), 320-329

Journal of Electrochemical Science and Technology
jecst.org

Li- and Na-ion Storage Performance of Natural Graphite via Simple Flotation Process

Noureddine Ait Laziz[1], John Abou-Rjeily[2], Ali Darwiche[3], Joumana Toufaily[4], Abdelkader Outzourhit[1], Fouad Ghamouss[2], and Moulay Tahar Sougrati[3]*

[1]*Laboratoire de Nanomatériaux pour l'énergie et l'environnement (LN2E)- Université Cadi Ayyad, Marrakech*
[2]*Faculté des Sciences, Laboratoire de Physico-Chimie des Matériaux et des Electrolytes pour l'Energie (PCM2E), Université François Rabelais, France*
[3]*Institut Charles Gerhardt, CNRS UMR 5253, Université de Montpellier, 34095 Montpellier Cedex 5, France*
[4]*Laboratory of Applied Studies for Sustainable Development and Renewable Energy (LEADDER); MCEMA, Lebanese University*

Abstract : Natural graphite is obtained from an abandoned open-cast mine and purified by a simple, eco-friendly and affordable beneficiation process including ball milling and flotation process. Both raw graphite (55 wt %) and its concentrate (85 wt %) were electrochemically tested in order to evaluate these materials as anode materials for Li-ion and Na-ion batteries. It was found that both raw and purified graphites exhibit good electrochemical activities with respect to lithium and sodium ions through completely different reaction mechanisms. The encouraging results demonstrated in this work suggest that both raw and graphite concentrates after flotation could be used respectively for stationary and embedded applications. This strategy would help in developing local electrical storage systems with a significantly low environmental footprint.

Keywords : Natural graphite, Na-ion batteries, Li-ion batteries, Energy storage, Stationary application, Froth flotation

Received : 20 July 2018, Accepted : 7 August 2018

1. Introduction

While some regions of the world are preoccupied with growing energy consumption, CO_2 emissions, and climate change, others are still suffering from the lack of conventional energy, particularly electricity, which penalizes their socio-economic development. This is particularly the case of around 18% of the world's population, living mostly in rural areas of South Asia and Sub-Saharan Africa [1]. Grid extension to such areas is not usually economically feasible. However, most of these regions are endowed with huge renewable energy (solar and/or wind) [2] as well as minerals resources. Consequently, investing in the harvesting and control of these energies would undoubtedly reduce the energy inequality and promote economic activities necessary for the improvement of the living conditions of a significant portion of populations living in these areas. The intermittence of renewables energies sources, which is one of the hurdles for their reliability and dispatchability, can be circumvented by the development of efficient and cost-effective energy conversion and storage systems. Electrochemical storage, a solution that has proven itself for embedded systems, may be adopted in this case provided that affordable materials not requiring expensive and extensive processing could be used.

Recently, our team (LN2E), evaluated the performance of a standalone solar photovoltaic power plant supplying electricity to the rural village Elkaria in the province of Essaouira - Morocco [3], where energy storage was provided by 24 lead-acid batteries. The choice of this technology for such small systems (some kWh) in isolated rural site is justified by the best compromise between performance and cost that it offers.

*E-mail address: Moulay-tahar.sougrati@umontpellier.fr
DOI: https://doi.org/10.5229/JECST.2018.9.4.320

Li-ion batteries are also among the candidate technologies for storage of clean electricity for such applications. However, despite their high reversibility and efficiency, they are still relatively expensive due to the materials and processes used in their fabrication. It is therefore very important to make this technology affordable to low-income populations by focusing on cost effective and naturally occurring materials that require only minimal physicochemical treatments.

Graphitic carbon is the most commonly used anode material in today's commercial lithium-ion batteries [4,5]. In fact, various forms of both synthetic and natural graphite have proven to be excellent lithium intercalation compounds [4,6]. Graphite has a theoretical specific capacity of 372 mAh/g [7], and depending on its type it can sustain a practical specific capacity more than 360 mAh/g [8]; which is close to theoretical limit. It also exhibits a low flat potential profile versus lithium and a good charge-discharge cycle stability which is considered to be one of the most important criteria for reliable and long-lived lithium-ion batteries [9,10].

On the other hand, despite its great success for Li-ion batteries, graphite exhibits a lower specific capacity when used as a Na-ion battery anode, because of its inability to form stable compounds with sodium [11,12]. However, Jache et al. discovered a new approach were graphite is capable of Na insertion and extraction via co-intercalation process with diglyme-based (diethylene glycol dimethyl ether) electrolytes [13]. This mechanism results in stage 1 ternary compound exhibiting excellent reversibility and superior cycle-life with a capacity close to 100 mAh/g. Subsequently, Kim et al reported a Na^+-solvent co-intercalation behavior in natural graphite using ether-based electrolyte [14].

The characteristics of synthetic graphite can be tailored in the manufacturing process making it the best choice for mobile applications. However, its cost is prohibitive for large-scale use such as in stationary storage infrastructures. As a consequence, natural graphite has emerged as an attractive alternative because of its low cost and its wide availability across the world. However, natural graphite requires beneficiation for obtaining desired grade for various end-uses. Various techniques can be applied to improve graphite grade including physical, chemical and thermal methods [15]. However, Because of natural hydrophobicity of graphite, flotation is the most used technique for its beneficiation [15]. In fact, a survey of literature indicates that graphite was the first mineral to be concentrated by flotation by Bessel Brothers in 1877 [15]. Thereafter, considerable advances in flotation were performed making it the economically competitive process to enrich mineral even low grade ore considered as waste [16]. It is thus not surprising that billions of tons of ore are beneficiated trough this technique annually. Furthermore, about 95% of the base metal produced are treated by flotation process [16]. Surprisingly, only a few studies focused on the purification and electrochemical performance of natural graphite in its raw and purified forms in the field of secondary batteries especially without the need of applying costly and time consuming purification methods. Most recently natural graphite was cycled vs. Li before using them as a source of graphene with a reversible capacity less than 200 mAh/g. The aim of this work is to study the possibility of making an electrochemical storage system from abundant and inexpensive minerals in Morocco. To this end, the electrochemical performances of naturally abundant graphite from an open-cast Moroccan mine as an anode material for Li-ion and Na-ion batteries were evaluated. This material is studied in its raw state and after a purification process using clean and low-cost process combining ball milling and flotation separation. To our knowledge, Moroccan natural graphite has never been studied in the field of secondary batteries. This abundant natural resource could potentially participate in a suitable development of the local economy. Moreover, Li/Na-ion technologies based on cheap materials are in line with the Moroccan strategy aiming at developing stationary storage systems for locally produced the green energy [24]. It is also important to note that this approach can contribute to reduce the negative impact on environment of the pollution due to abandoned mining sites as evidenced in recent studies [25,26].

2. Experimental

Samples of Moroccan natural graphite were obtained from the abandoned Sidi Bou Othmane open-cast mine located 33 kilometers north of Marrakesh city (Morocco). This region was also operated for Pb, Zn, and pyrite extraction until 1980 [27].

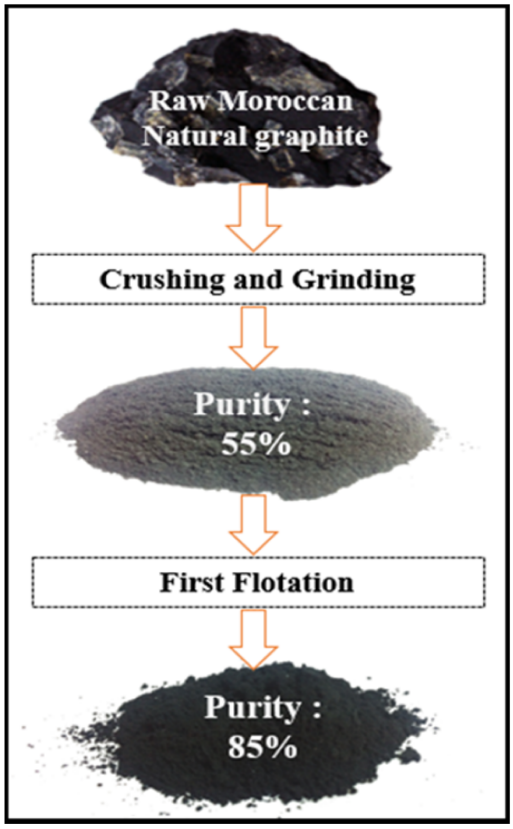

Fig. 1. Simplified scheme illustrating the purification process of natural graphite.

Successive processes were carried out to purify these natural samples (Fig. 1). First, the samples were crushed and sieved in order to obtain powders with uniform grain size. Subsequently, the powders were subjected to wet grinding in a ball mill for 10 minutes. The first flotation purification process was then performed in a 5 liters cell. The froth flotation process used here is a simplified form of the method reported by Vasumathi et al. [22]. Tap water and a few drops of commercial grade MIBC (Methyl Isobutyl Carbinol) frother were used. As a result, the hydrophobicity of graphite and its low density compared to other metallic impurities enables its separation and collection from the top of the flotation cell (Fig. 1). The floatation residue is collected and stored for further characterization.

The chemical composition of the graphite at each step were determined by using X-ray fluorescence (PANalytical AXIOS max). All the concentrations given below are in wt%. X-ray diffraction (XRD) analysis was performed using an X'Pert diffractometer (PANalytical) to identify the main crystalline phases of the raw and purified graphite. Scanning electron microscopy (SEM) coupled with energy-dispersive X-ray spectroscopy (EDS) analysis (Samx machine) where used to examine the morphology and the elemental composition of the obtained powders.

Raman spectroscopy was carried out using a green laser at 532 nm. The thermogravimetric analysis (TGA) was performed under air with a heating rate of 5°C/minute from 20 to 950°C. The specific area was determined by nitrogen adsorption/desorption method at 77 K using a Quantachrome apparatus (QUADRASORB Evo). The specific surface was obtained by applying the Brunauer, Emmett, Teller (BET) model.

Electrochemical characterization of the raw graphite and its concentrate were performed on CR2032 coin-type cells at 25°C. The working electrode was prepared using a mixture of graphite powder, superconductive carbon (carbon black), and polyvinylidene difluoride (PVDF) as a binder with a weight ratio of 70:22:8 respectively. The mixture was ball milled with N-Methyl-2-pyrrolidone (NMP) to form the slurry which was cast on copper foils and dried under vacuum at 80°C overnight. The final mass loading of the active material on the electrode was almost the same between raw graphite and its concentrate (1.5 to 2 $mg.cm^{-2}$). For sodium-ion batteries PVDF, NMP and copper foil were substituted with carboxymethylcellulose (CMC), distilled water and an aluminum foil respectively.

The coin cells were assembled inside an argon-filled glove box using lithium or sodium foils as counter electrodes and a borosilicate glass microfiber sheet (Whattman) as a separator. The organic electrolyte used was made by dissolving $LiPF_6$ (1M) in a (1 : 1% wt) solution of ethylene carbonate (EC) and dimethyl carbonate (DMC) then 5% fluoroethylene carbonate (FEC) was added as an additive for lithium-ion batteries. Whereas for sodium-ion batteries, the organic electrolyte was composed of 1M $NaPF_6$ dissolved in diglyme.

Cyclic voltammetry (CV) was conducted with a 25 $\mu V \cdot s^{-1}$ scanning rate and the potential was recorded versus Li/Li+ starting from the open-circuit voltage (ranging from 2.6 to 3 V) and ending at 0.02 V. The cut-off voltages for constant current

charge/discharge were respectively 2 V/ 0.02 V for lithium and 2 V/0.005 V for sodium-ion batteries. All electrochemical tests were conducted on a multichannel potentiostat, VMP (BioLogic). Specific capacity and gravimetric current are reported with respect to the active mass of the active materials (raw and graphite concentrate) in the electrodes.

3. Results and Discussion

3.1. Physical and chemical analyses

The average chemical compositions of raw and purified graphite obtained by X-ray fluorescence are given in Table 1 (Elements with less than 0.1% concentrations were neglected). This simple purification process enhanced the purity of the samples from 55.2% to 85%. The increase of carbon content is accompanied with a net decrease of the other chemical elements (O, Ca, Si, Al) which are associated to graphitic carbon as impurities. It is worth noting that the studied graphite does not contain any heavy or toxic metals; the heaviest detected metal is iron. Therefore, the flotation residues are composed of non-toxic materials.

The results of the XRF analysis were further confirmed by TGA measurements (Fig. 2), The weight loss of the samples could be attributed to the reaction of carbon with oxygen leading to the release of CO_2: The results revealed a carbon content of 50% and 86% for the raw and the flotation concentrate samples respectively. The minor increase in mass observed below 400°C is mainly attributed to the reaction of some elements with oxygen.

Fig. 3 (a-b) show SEM images of raw and concentrate graphite agglomerates. EDS elemental qualitative analysis of the raw graphite powder shows regions with a mixture of carbon and silicon impurities and small peaks corresponding to aluminum and magnesium. In contrast to raw graphite, traces of calcium and iron were present in the graphite concentrate. Their absence in raw graphite EDS can be attributed to the random sampling and zone selection.

Fig. 4 represents Raman spectra of raw graphite and graphite concentrate respectively. Raman spectra provide a direct evaluation of the graphitization

Table 1. Chemical composition (wt %) of raw graphite and graphite concentrate after flotation obtained by X-ray Fluorescence (XRF).

	C	O	Ca	Si	Fe	Al	Mg
Raw Graphite (wt%)	55.2	24.5	8.4	7.5	1.3	1.7	0.8
After Flotation (wt%)	84.8	7.67	1.7	2.7	1.7	0.3	0.6

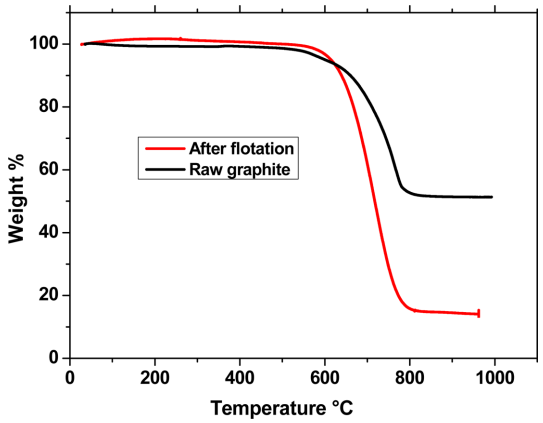

Fig. 2. TGA analyses of raw graphite (Black line) and flotation concentrate (Red line) under air.

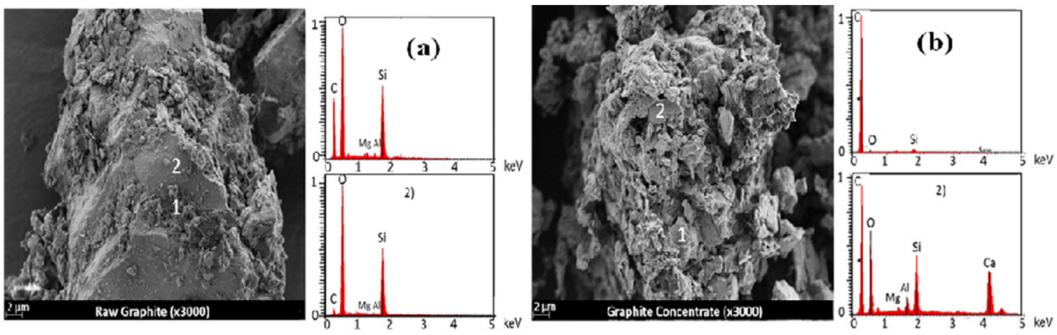

Fig. 3. SEM images of raw graphite powder (a) and Graphite concentrate powder (b) with EDS analysis for two spots (1 and 2) shown in the images.

degree of carbonaceous materials using the intensity ratio of the D (1340 cm^{-1}) and G bands (around 1575 cm^{-1}) [28]. The low-intensity ratios (I_D/I_G = 0.19 and 0.15 respectively for raw and concentrated graphite) indicates a high degree of graphitization. The decrease of the I_D/I_G after flotation suggests a partial removal of small and less graphitized carbon particles not liberated from the gangue in the ball milling operation. Raw graphite spectra showed additional bands that can be attributed to the presence of impurities, which are mostly quartz, with Raman shift peaks at 134, 172, 272 (strong), and 508 cm^{-1} [29,30], almandine at 239, 367 (strong), 541, 818 and 874 cm^{-1} (very strong) [31], and finally calcite at 272 (strong), and 1080 cm^{-1} (very strong) [32]. Nevertheless, after flotation, these impurity peaks have significantly diminished, therefore evidencing the high efficiency of the floatation treatment.

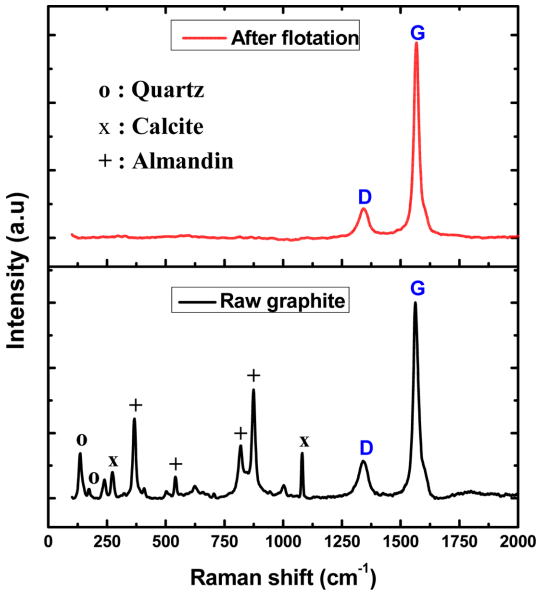

Fig. 4. Raman spectra of raw graphite (bottom) and concentrate graphite (top).

Fig. 5, shows the X-ray diffraction patterns of raw graphite and flotation concentrate. In the case of raw natural graphite, in addition to the graphite peaks (G) occurring at around 26.48°, the most intense diffraction peaks indicated with (x) are attributed to the calcite $CaCO_3$. Quartz and almandine phase $Ca_3Al_{1.6}Fe_{0.4}(SiO_4)_3$ indicated with (o) and (+) respectively can also be easily distinguished. It is worth noting that the diffraction intensities are not only proportional to the phase content, but also to the electronic density, which is very high in the case of heavy elements compared to carbon. This explains, for example, the high intensity of almandine and calcite peaks compared to graphite ones. After flotation, the characteristic peaks of graphite occurring at 26.48° becomes clearly more intense suggesting the drastic decrease of the amount impurities, especially calcite and almandine. The efficiency of flotation for calcite and almandine removal is a consequence of the synergistic effect of their high densities (4.31 g/cm^3 and 2.71 g/cm^3 respectively), compared to graphite (2.26 g/cm^3), and the hydrophobicity difference of the materials.

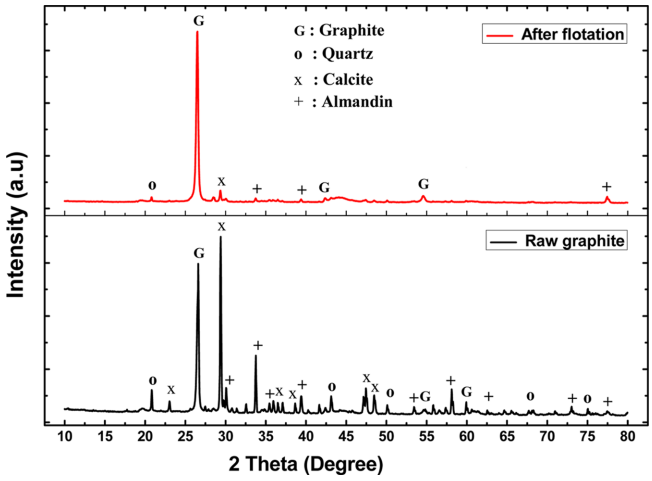

Fig. 5. XRD patterns of raw graphite (bottom) and concentrate graphite (top). (Cu-Kα)

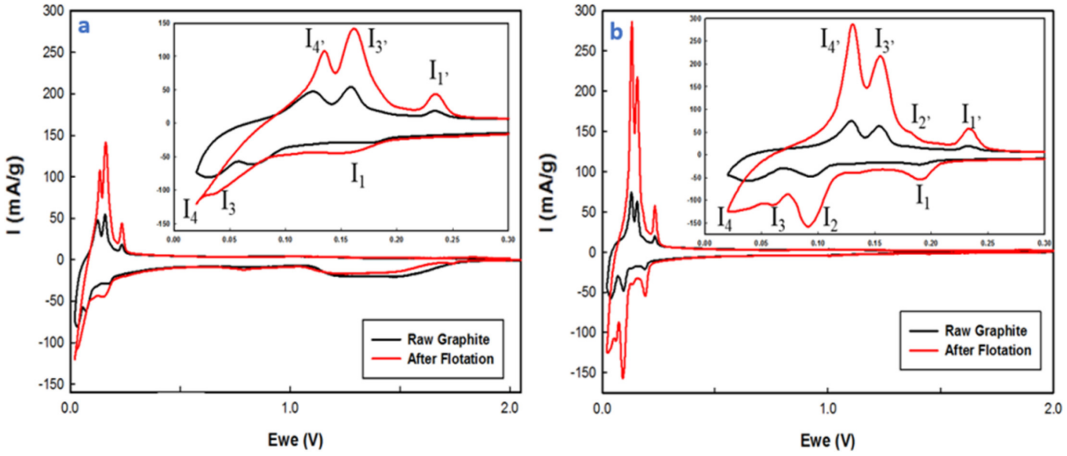

Fig. 6. Cyclic voltammetry of raw graphite (black) and concentrate (red) vs. Li. In the (a) 1st cycle and (b) 3rd cycle. Insets give zooms on the graphite reaction voltage range.

The specific surface area analysis of graphite in its raw and flotation concentrate forms were carried out via nitrogen adsorption/desorption. The specific surface area determined from the BET model increases from 10.4 to 16.6 m^2/g after flotation. These values, of high significance for electrochemical performance, are in the range of reported data for both natural and synthetic graphite [4].

3.2. Electrochemical performance

Cyclic voltammetry (CV) measurements vs. lithium during the first and third cycle, are shown in fig. (6-a, b) for raw and concentrated graphite. The general shape of the voltammograms for both raw graphite and flotation concentrate are similar to the reported data [33]. During the first lithiation, a broad reduction peak is observed in the voltage region of 1.7 V to 1.075 V. This peak is attributed to the SEI (solid electrolyte interphase) formation mainly as a result of electrolyte decomposition [33]. The lithium intercalation reaction starts from 0.25 V vs. Li, in accordance with previous studies [21]. During the first cycle, only three graphite lithiation reactions are evident during the back scan of the voltage for raw graphite (stage III (I2) is not evident), whereas the flotation concentrates show all the four expected reactions. These peaks correspond to the following reactions: stage IV (I1) reaction yielding LiC_{24}, stage III (I2) reaction yielding LiC_{18}, stage II (I3) reaction yielding LiC_{12} and stage I (I4) yielding fully intercalated graphite with LiC_6 [34]. Fig. 6-b shows the 3rd CV cycle where it can be clearly seen that the previously observed reduction peaks between 1.70 V and 1.075 V in Fig. 6-a have drastically decreased for raw graphite and almost disappeared for graphite concentrate. This observation indicates that the SEI layer formation took place mainly during the first CV cycle. Furthermore, at a low potential, as expected, the different stages of lithium intercalation designated as (I1, I2, I3, and I4) are evident in both electrodes. It is worth noting that after flotation, the gravimetric current is much higher than for raw graphite suggesting a higher rate of lithiation in the graphite lattice. This can be attributed to a higher graphitic carbon content of the material after flotation, which is in perfect agreement with XRD, XRF, SEM, TGA and Raman observations.

Both samples were cycled at a current density rate of C/20. The gravimetric current during the charge/discharge experiment was calculated with respect to the theoretical specific capacity of graphite vs. lithium (372 mAh/g). As shown in Fig. 7-a, during the first electrode lithiation, there is a significant contribution of the electrolyte reduction on the delivered capacities between open-circuit voltage and 0.2 V. The graphite lithiation occurs in the voltage range extending from 0.2 V to 0.02 V vs. Li. The results show that graphite concentrate has a higher reversible capacity compared to raw graphite. Raw graphite attained a maximum reversible capacity of 150 mAh/g, whereas after flotation this capacity was doubled reaching about 300 mAh/g. This difference in revers-

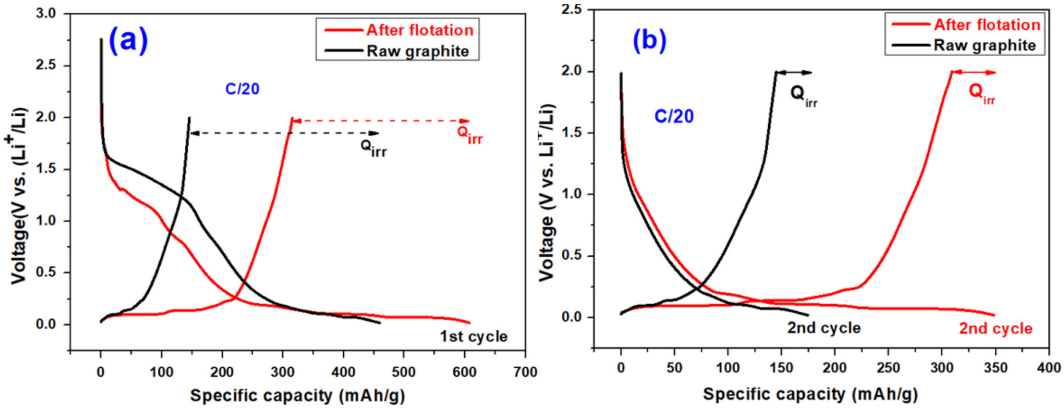

Fig. 7. Galvanostatic profiles of raw (black) and concentrate (red) graphite vs. Li at a current density rate of C/20. (a) First cycles and (b) Second cycles.

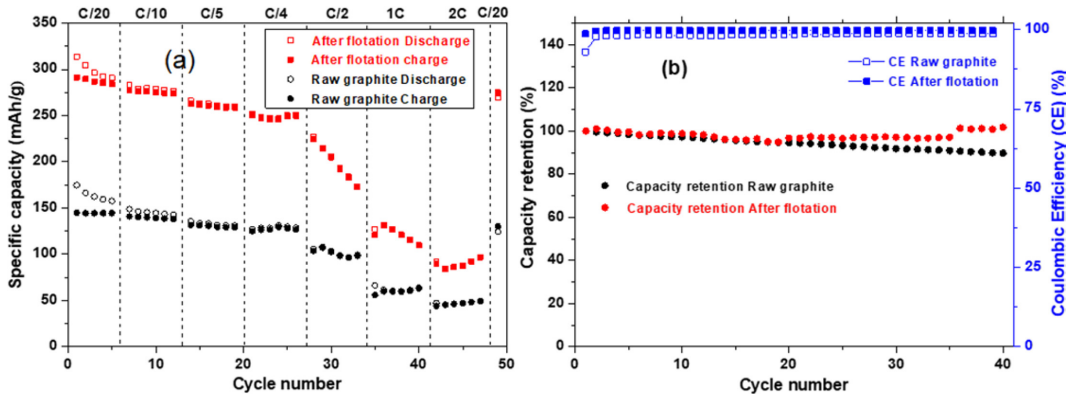

Fig. 8. (**a**) Rate capabilities for raw (black) and concentrated graphite (red). (b) Capacity retention (%) and coulombic efficiency at C/5 vs. Li.

ible capacity can be attributed to the differences in inactive materials contents, particle size and the specific surface area as it was previously evidenced by XRD, SEM and BET analyses.

In the second charge/discharge cycles depicted in Fig. 7-b, both samples show similar behavior as reduction occurs from 2 V to 0.2 V during the lithiation, yielding a specific capacity of 77 mAh/g for raw graphite and 96 mAh/g for graphite concentrate. This "high voltage" capacity is recovered during the following discharge cycles. Furthermore, the potential range, as well as the sloping voltage profile of the charge/discharge curve between 2 and 0.2 V, could indicate that this capacity is not due to lithium intercalation in graphitic carbon. The existence of amorphous/disordered carbon or more generally non-graphitized carbon may explain this sloping charge/discharge profile between 2 V and 0.02 V contrasting with the typical steeper slopes of charge/discharge curves of graphite [35]. Similar high voltage charge/discharge profiles are usually observed for non-graphitic carbon materials [36]. In raw graphite, the total charge capacity in the second cycle reached 145 mAh/g and 291 mAh/g for graphite concentrate. As a conclusion, flotation was able to considerably reduce impurities and allow more graphitic carbon to be exposed to lithiation and de-lithiation.

Electrochemical rate capabilities at C/20, C/10, C/5, C/4, C/2, 1C, and 2C are shown in Fig. 8-a. In both samples, a small fading in capacity was observed when the C-rate was varied from C/20 to C/4. The capacity fading becomes more significant as the bat-

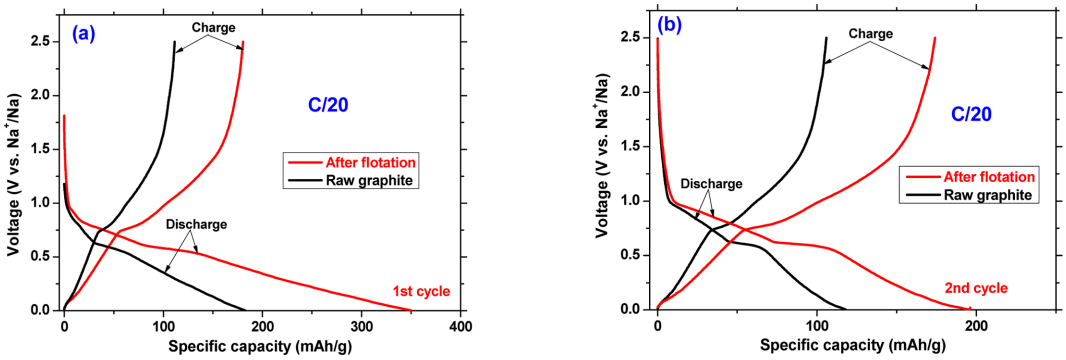

Fig. 9. (**a**) First and (b) second galvanostatic cycles of raw (black) and concentrated (red) graphite vs. Na.

tery undergoes faster cycling regimes (from C/2 to 2C). Furthermore, for both materials, the capacity is recovered when cycling again at the C/20 rate. This indicates that the capacity losses are attributed to the kinetics of the reactions and not to degradation of the materials. It is also worth noting that for raw graphite, the stabilization and the complete formation of the SEI layer take place around the 15th cycle, where irreversibility was diminished. Whereas, stabilization and complete formation of the SEI layer for graphite concentrate took place earlier on the 6th cycle. This can be explained by the decreased amount of impurity that likely delays the formation of a homogenous SEI. Stability tests were performed under constant charging/discharging current and the results are depicted in Fig. 8-b. For raw graphite, an acceptable capacity retention and an average C/C_0 (C is charge capacity for a given cycle, and C_0 is charge capacity of the second cycle) reaching 0.94 was obtained after 40 cycles. In addition, stable cycling was noticed with a reasonable coulombic efficiency of 98.3%. For graphite concentrate, a higher capacity and increased stability and efficiency were noticed, C/C0 = 0.98 and a coulombic efficiency of to 99.7%. Nevertheless, a serious limitation that needs to be tackled of both raw and concentrated graphite is the low coulombic efficiency during the first 15 cycles.

A preliminary study aiming to evaluate the electrochemical activity of our materials vs. sodium was also conducted. Fig. 9, shows the galvanostatic profiles for raw graphite and concentrate, using diglyme electrolyte containing $NaPF_6$ (1M) salt. The first sodiation profiles show similar shapes but different capacities. During the first sodiation (Fig. 9-a), raw graphite delivered a capacity of around 180 mAh/g,

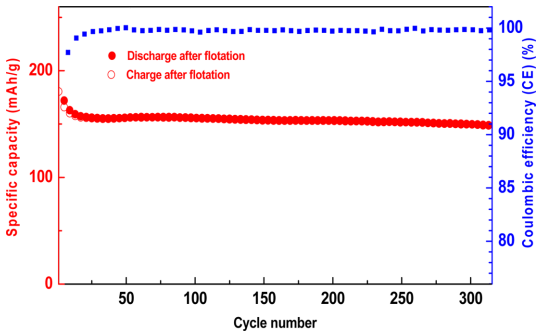

Fig. 10. Cycling stability of natural graphite (Raw and concentrate graphite) vs. Na.

while graphite concentrate reached values of around 351 mAh/g. Desodiation capacities of ~110 mAh/g and ~180 mAh/g were obtained for raw graphite and graphite concentrate respectively.

During the second galvanostatic cycle of Fig. 9-b, raw graphite shows a sodiation capacity of ~118 mAh/g and a desodiation capacity of ~105 mAh/g, while graphite concentrate shows a sodiation capacity of ~196 mAh/g and a desodiation capacity of ~174 mAh/g. The latter value is significantly higher than those found by Jache et al. (100 mAh/g) [13] and Kajita et al. (110 mAh/g) [37]. It is worth noting that the loss of capacity between the charge and discharge is mainly attributed to the continuous electrolyte reduction during the second cycle.

Cycling stability vs. Na of raw and concentrate materials was investigated at cycling rate of C/20 as shown in Fig. 10, both raw and concentrate graphite exhibit good cycling stability with coulombic efficiencies approaching 100% after 15 cycles. Furthermore, raw graphite provides a capacity close to

95 mAh/g after 50 cycles, while concentrate graphite provides a capacity close to 150 mAh/g after 300 cycles with very low capacity decay rate of 0.02% per cycle from the 15th cycle to 300th cycle. The excellent cycle stability of raw and concentrate graphite suggests that although the presence of impurities limits the specific capacity it does not significantly affect the cycle life of the studied materials.

4. Conclusions

Despite the presence of some impurities in the raw Moroccan natural graphite, this primary electrochemical evaluation reveals its good electrochemical capabilities versus both lithium and sodium. The cycling stability in both Li and Na half cells seems to not be significantly affected by the presence of these impurities though it limits the useful specific capacity. The simple purification process (ball milling and flotation) successfully increased the purity of the raw graphite from 55% to 85%. Relatively good stability at fast cycling rates was achieved with a room of improvement by optimizing the ball milling and the flotation processes.

The possibility of a commercial valorization could be achieved depending on the intended use. The raw natural graphite could be used for stationary electrochemical storage of the locally produced electrical energy (stationary system) whereas the purified graphite can be used for embedded applications as advanced chemical/physical treatments are required to further improve its quality. This approach can be completed if the widely available Moroccan phosphate is used to produce $LiFePO_4$ cathode materials.

Acknowledgment

This work is in appreciation for the Lebanese government for providing student scholarships for one of the authors (J. A-R) and Mr. Pierre-Ivan Raynal for the SEM observations.

Author Contributions

N.A.L. was responsible for material collection, purification, electrochemical characterization and is a primary author, J.A-R. was responsible for chemical, physical, and electrochemical characterization and is a secondary author, M.T.S. provided supervision, scientific advisory along with XRD characterization, A.D. performed electrochemical characterization along with scientific advisory, J.T. was also a scientific advisor and an English proofreader for this article, A.O. provided scientific advisory along with supervision, finally F.G. was the supervisor of this project along with its management, consultation, and proofreading.

Conflicts of Interest

"The authors declare no conflict of interest." "The founding sponsors had no role in the design of the study; in the collection, analyses, or interpretation of data; in the writing of the manuscript, and in the decision to publish the results".

References

[1] G. Zubi, R. Dufo-López, N. Pardo, G. Pasaoglu, *Energ. Convers. Manag*., **2016,** *122,* 439-448.
[2] Geographical Assessment of Solar Resource and Performance of Photovoltaic, Technology Joint Research Centre, European Commission (PVGIS), **2016**.
[3] A. El Fathi, L. Nkhaili, A. Bennouna, A. Outzourhit, *Energ. Convers. Manag*., **2014**, *86*, 490-495.
[4] M. Herstedt, L. Fransson, K. Edström, *J. Power Sourc*., **2003**, *124(1)*, 191-196.
[5] K.A. Striebel, A. Sierra, J. Shim, C.-W. Wang, A.M. Sastry, *J. Power Sourc*., **2004**, *134(2)*, 241-251.
[6] J. Park, S.S. Park, Y.S. Won, *Electrochim. Acta*, **2013**, *107*, 467-472.
[7] S. Megahed, B. Scrosati, *J. Power Sourc*., **1994**, *51(1-2)*, 79-104.
[8] H. Zhao, J. Ren, X. He, J. Li, C. Jiang, C. Wan, *Solid State Sci*., **2008**, *10(5)*, 612-617.
[9] K. Zaghib, X. Song, A. Guerfi, R. Rioux, K. Kinoshita, *J. Power Sourc*., **2003**, *119*, 8-15.
[10] Z. Yang, J. Zhang, M.C.W. Kintner-Meyer, X. Lu, D. Choi, J.P. Lemmon, J. Liu, *Chem. Rev*., **2011**, *111(5)*, 3577-3613.
[11] J. Sangster, *JPED*, **2007**, *28*, 571-579.
[12] K. Nobuhara, H. Nakayama, M. Nose, S. Nakanishi, H. Iba, *J. Power Sourc*., **2013**, *243*, 585-587.
[13] B. Jache, P. Adelhelm, Angew. *Chem. Int. Ed*., **2014**, *126(38)*, 10333-10337.
[14] H. Kim, J. Hong, Y. Park, J. Kim, I. Hwang, K. Kang, *Adv. Funct. Mater*., **2015**, *25(4)*, 534-541.
[15] S. Chehreh Chelgani, M. Rudolph, R. Kratzsch, D. Sandmann, J. Gutzmer, *Min. Proc. Extr. Metal. Rev*., **2016**, *37*, 58-68.
[16] M.C. Furstenau, G. Jameson, R. Yoon Eds, in "Froth Flotation a Century of Innovation" Publisher: Society for

Mining, Metallurgy, and Exploration, **2007**.
[17] M. Hochberg Renewable Energy Growth in Morocco. Available from: https://www.mei.edu/sites/default/files/publications/PF26_Hochberg_Moroccorenewables_web.pdf.
[18] A. EL Gharmali, (Ph.D. thesis) Marrakech, Morocco: University Cadi Ayyad, **2000**.
[19] Y. Taha, M. Benzaazoua, R. Hakkou, M. Mansori, Miner. Eng., **2017**, *107*, 123-138.
[20] S. El Baz, M. Baz, M. Barakate, L. Hassani, A. El Gharmali, B. Imziln, *Sci. World J.*, **2015**, *2015*, 731834.
[21] L. Bokobza, J.-L. Bruneel, M. Couzi, *C*, **2015**, *1(1)*, 77-94.
[22] P. Gillet, A. Le Cléac'h, M. Madon, *JGR: Solid Earth*, **1990**, *95(B13),* 21635-21655.
[23] D. Krishnamurti, *Proc. Indian Acad. Sci*., **1958**, *47*, 276-291.
[24] T. Ganetsos, T. Katsaros, P. Vandenabeele, S. Greiff, S. Hartmann, *Int. J. Chem. Mater. Res*., **2013**, *3*, 5-9.
[25] S. Gunasekaran, G. Anbalagan, S. Pandi, *J. Raman Spectrosc*., **2006**, *37(9)*, 892-899.
[26] M. Nie, J. Demeaux, B.T. Young, D.R. Heskett, Y. Chen, A. Bose, J.C. Woicik, B.L. Lucht, *J. Electrochem. Soc*., **2015**, *162(13)*, A7008-A7014.
[27] M. Yoshio, H. Wang, K. Fukuda, Y. Hara, Y. Adachi, *J. Electrochem. Soc*., **2000**, *147(4)*, 1245–1250.
[28] E.M.C. Jones, Ö.Ö. Çapraz, S.R. White, N.R. Sottos, *J. Electrochem. Soc*., **2016**, *163(9)*, A1965-A1974.
[29] M. Yoshio, R.J. Brodd, A. Kozawa, eds., Lithium-Ion Batteries: Science and Technologies, Springer-Verlag, New York, **2009**.
[30] M. Endo, C. Kim, K. Nishimura, T. Fujino, K. Miyashita, *Carbon*, **2000**, *38(2)*, 183-197.
[31] T. Kajita, T. Itoh, *Phys. Chem. Chem. Phys*, **2017**, *20*, 2188-2195.